Polymer Chemistry

Accepted Manuscript

ROYAL SOCIETY OF CHEMISTRY

www.rsc.org/polymers

Journal Name

RSCPublishing

ARTICLE

Influences of the Backbone Randomness to the Properties, Morphology and Performances of the Fluorinated Benzoselenadiazole-Benzothiadiazole Based Random Copolymers

Cite this: DOI: 10.1039/x0xx00000x

Received 00th January 2012,
Accepted 00th January 2012

DOI: 10.1039/x0xx00000x

www.rsc.org/

Yung-Tsung Chen, Tzu-Wei Huang, Chien-Lung Wang,* and Chain-Shu Hsu*

To investigate the influences of the 5,6-difluoro-benzoselenadiazole: 5,6-difluoro-benzothiadiazole (FBSe:FBT) ratio to the polymer properties, solid-state morphology and device performances, a series of FBSe:FBT based copolymers were synthesized. Copolymers with higher FBSe ratios were found to have narrower E_g, and higher-lying E_{HOMO}. Because of the size and electronegativity differences of the selenium and sulfur atoms, the FBSe:FBT ratio further affects the structural regularity of the conjugated chains, and their self-assembly behaviors. DSC results indicated that P1, which has the most irregular FBSe:FBT sequence along the backbone showed the lowest T_m. Interestingly, XRD results showed that the main-chain irregularity degrades the order of the lamellar stacking, but not the order of π-stacking. The random ternary copolymers, P1 and P2, possess more ordered π-stacking than the alternating copolymers, PTh_4FBSe and PTh_4FBT. The highest OFET μ_h of 0.46 $cm^2 V^{-1}s^{-1}$ was delivered by P1, which has the smallest $d_{\pi-\pi}$ among the copolymers. In the polymer:$PC_{71}BM$ blend films, the FBSe containing copolymers have good miscibility to $PC_{71}BM$. The degree of phase separation of PTh_4FBSe:$PC_{71}BM$ can be enhanced by DIO additive, but it is not effective for the random ternary copolymers. Highest PCE of 6.06% with V_{oc} of 0.64 V, J_{sc} of 15.3 mA/cm^2, and FF of 61.8% were delivered by the PTh_4FBSe:$PC_{71}BM$ PSCs.

Introduction

Low band-gap (LBG) conjugated copolymers consisting of electron-rich donor unit (D) and electron-deficient acceptor unit (A) have been developed as high-performance materials used in bulk heterojunction (BHJ) polymer solar cells (PSCs).[1-5] Rapid developments in the polymer design enabled the adjustments of the highest occupied molecular orbital level (E_{HOMO}) and lowest unoccupied molecular orbital level (E_{LUMO}) of the LBG copolymers. Combining the suitable E_{HOMO} and E_{LUMO} of the LBG copolymer, appropriate device design and morphological optimization, BHJ PSCs have reached power conversion efficiencies (PCEs) over 8%.[6-19]

Recently, random copolymerization has been developed as a versatile strategy to further adjust the properties of D-A copolymers. The D-A random copolymers were generally prepared either by copolymerizing two different D units with one A unit[19-22], or by copolymerizing two different A units with one D unit.[23-29] Compared to the alternating D-A copolymers, which contain only two monomeric units, the additional monomeric units in the ternary random copolymers provide extra flexibility to adjust the polymer properties. Different ternary random copolymers have been synthesized to either broaden absorption spectrum,[19] modulate the E_{HOMO}, E_{LUMO} positions,[23] or to control the solid-state morphology.[22] Over 7 % PCEs have been reported in the single-junction BHJ PSCs of several random D-A copolymers, and PCE of over 8.5% has also been reported in our previous study using the prophyrin-containing random copolymers.[19]

Although the versatility of the random copolymerization has been confirmed, because the reaction brings both the irregularity to the chemical structure and the randomness to chain sequence along the conjugated backbone, fundamental questions about how these molecular parameters influences the solid-state morphology and device performances of the random D-A copolymers remains an interesting issue to be explored. A suitable acceptor pair for the study of the influences of the backbone randomness is fluorinated benzothiadiazole (FBT) and fluorinated benzoselenadiazole (FBSe). Unlike most ternary random copolymers containing two A units with very different structures, because FBSe and FBT have very similar chemical structures. Thus, when randomly copolymerized, the overall chemical structure of the random copolymers will not be significantly altered with the FBSe:FBT ratios. However, because the selenium atom (Se) and the sulfur atom (S) are different in their electronegativity and sizes,[30-35] changing the FBSe:FBT ratio in the ternary random copolymers can still change the polymer properties and bring the sequential randomness into the conjugated backbone. In general, the FBSe-based copolymers[36-38] have smaller E_g,[39-42] but higher-lying E_{HOMO} than the FBT-based copolymers,[43-46] because the Se-containing unit is more polarized than its S analogue and possesses more quinoidal character.[47] Currently, the FBSe-based copolymers have delivered a promising PCE of 5.74% in the literature. Adjusting the FBT/FBSe ratio in a ternary random copolymer may optimize the polymer properties, and provide information about how the backbone randomness affects the solid-state structures of the random copolymers. Thus, in this study, a series of LBG copolymers, which contains FBSe and FBT as a pair of A units and 5,5′-dibromo-4,4′-bis(2-octyldodecyl)-2,2′-

bithiophene as D unit, were synthesized to investigate the influences of the FBSe:FBT ratio to the polymer properties, solid-state behaviors and device performances. As shown in Scheme 1, the FBSe:FBT ratios are 100:0 for PTh_4FBSe, 50:50 for P1, and 25:75 for P2. UV-Vis spectra and electrochemical cyclic voltammetry (CV) were used to evaluate influences of the FBSe:FBT ratio on the E_{HOMO}, E_{LUMO} and E_g. The phase behavior and phase structure of the copolymers were investigated by differential scanning calorimetry (DSC) and X-ray diffractometer. The morphology of the copolymer/PCBM blend films and the influences of the diiodooctane (DIO) additive were observed by transmission electron microscopy (TEM). The FBSe:FBT ratio showed obvious influences to the properties and solid-state morphologies of the copolymers. The highest OFET hole mobility (μ_h) of 0.46 $cm^2 V^{-1}s^{-1}$ was delivered by P1, which has the smallest $d_{\pi-\pi}$; while the highest PCE of 6.06 % with V_{oc} of 0.64 V, J_{sc} of 15.3 mA/cm^2, and FF of 61.8% were delivered by the PTh_4FBSe:$PC_{71}BM$ PSCs because of the suitable degree of phase segregation in the blend thin film.

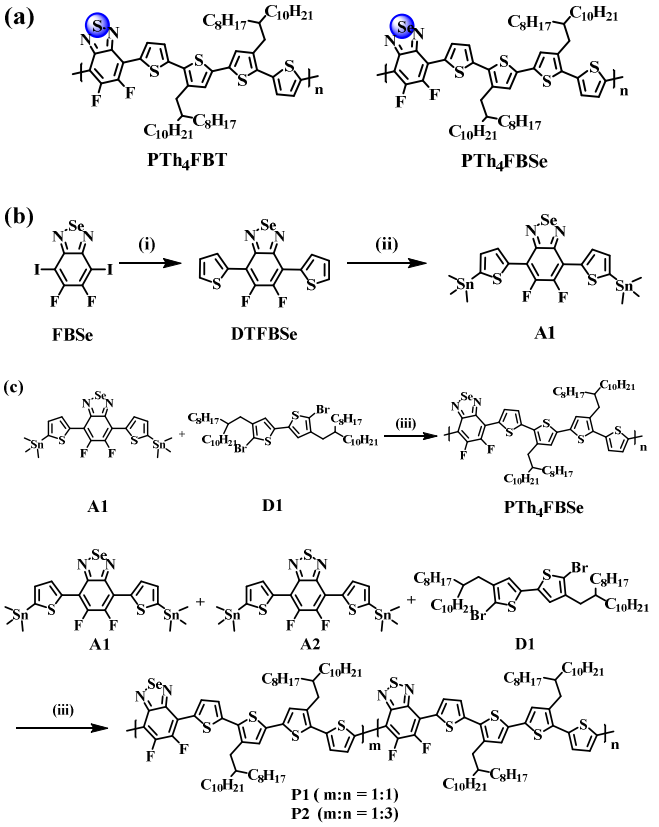

Scheme 1 (a) Chemical structures of PTh_4FBT and PTh_4FBSe. (b), (c) Synthetic procedures and conditions of the monomers and copolymres: (i) 2-(tributylstannyl)thiophene, tetrakis (triphenylphosphine)palladium(0), DMF, 120 °C, 24hr; (ii) LDA, dry THF, − 78 °C, 1 hr; 1 M trimethyltin chloride; (iii) tris(dibenzylideneacetone)dipalladium(0), tri(o-tolyl)phosphine, chlorobenzene, 180 °C, microwave 270 W, 50 mins.

Experimental Section

General Measurement and Characterization: All chemicals are purchased from Aldrich, Lancaster, TCI or Acros used as received unless otherwise specified. ^1H and ^{13}C NMR spectra were measured using a 400 and 75 MHz instrument spectrometer. Differential scanning calorimetry (DSC) was performed on a TAQ200 Series DSC and operated at a scan rate of 10 °C min^{-1}. Thermogravimetric analysis (TGA) was recorded on a Perkin Elmer Pyris under nitrogen atmosphere at a heating rate of 10 °C/min. UV-Vis spectra were measured using an HP 8453 spectrophotometer.The electrochemical cyclic voltammetry (CV) was conducted on a CH Instruments Model 611D. A Carbon glass coated with a thin polymer film was used as the working electrode and Ag/Ag^+ electrode as the reference electrode, while 0.1 M tetrabutylammoniumhexafluorophosphate (Bu_4NPF_6) in acetonitrile was the electrolyte. CV curves were calibrated using ferrocence as the standard, whose oxidation potential is set at −4.8 eV with respect to zero vacuum level. The E_{HOMO} were deduced from the equation $E_{HOMO} = -e(E_{ox}^{onset} - E_{(ferrocene)}^{onset} + 4.8)$ eV. The E_{LUMO} levels of polymer were deduced from the equation $E_{LUMO} = -e(E_{red}^{onset} - E_{(ferrocene)}^{onset} + 4.8)$ eV. For X-ray diffraction (XRD) patterns, Bruker APEX DUO Single Crystal X-Ray Diffractometer with a microfocus air-cooled sealed Cu tube source, 50 watts, (50 kV, 1 mA; K_α radiation 0.1542 nm) and an APEXII CCD camera was used. For the 2D WAXD analysis, the fiber samples were prepared by extruding the polymers through a pin-hole (diameter:1 mm) at xx °C. The fiber samples were then exposed to the X-ray (beam size: 0.3 mm). The exposure time to obtain high-quality patterns was 40 seconds.

OFET Device Fabrication and Characterization: An *n*-type heavily doped Si wafer with a SiO_2 layer of 300 nm and a capacitance of 11 nF/cm^2 was used as the gate electrode and dielectric layer. Thin films (40–60 nm in thickness) of polymers were deposited on ODTS treated SiO_2/Si substrates by spin-coating their *o*-DCB solution (5 mg/mL). The thin films were annealed at 200 °C or 250 °C for 10 minutes. Gold source and drain contacts (40 nm in thickness) were deposited by vacuum evaporation on the organic layer through a shadow mask, affording a bottom-gate, top-contact OFET device. Electrical measurements of the OFET devices were carried out at room temperature in air using a 4156C Semiconductor Parameter Analyzers, Agilent Technologies. The field-effect mobility was calculated in the saturation regime by using the equation, $I_{ds} = (\mu WC_i/2L)(V_g - V_t)^2$, where I_{ds} is the drain-source current, μ is the field-effect mobility, W is the channel width (1 mm), L is the channel length (0.1 mm), C_i is the capacitance per unit area of the gate dielectric layer, V_g is the gate voltage and V_t is threshold voltage.

BHJ PSC Fabrication and Characterization: The device structure for inverted PSCs was ITO/ZnO/Polymer: $PC_{71}BM/MoO_3$/Ag. The ITO glass substrates were cleaned with detergent, deionized water, acetone, and isopropyl alcohol in an ultrasonic bath and then dried overnight in an oven at >100 °C. For the inverted PSCs, Zinc acetate dihydrate (Aldrich) dissolved in 2-methoxyenthanol (100 mg mL^{-1}) and small amount of ethanolamine was spin-casted on pre-cleaned ITO substrates and baked at 160 °C for 10 minutes in the air to form the ZnO layer with thickness of 40 nm. Copolymers were dissolved in chlorobenzene (CB) containing 3 v% DIO. $PC_{71}BM$ (purchased from Nano-C) was then added into the solution to reach the desired weight ratio. The solution was stirred at 70 °C for overnight and filtrated through a 0.45um filter. In a glove box, the solution of polymer:$PC_{71}BM$ was then spin coated to form the active layer. The anode made of MoO_3 (7 nm) and Ag (150 nm) was evaporated through a shadow mask under vacuum (<10^{-6} Torr). Each sample consists of four independent pixels defined by an active area of 0.04 cm^2. The devices were characterized in air under 100 mW/cm^2 AM 1.5

simulated light measurement (Yamashita Denso solar simulator). Current−voltage (*J*−*V*) characteristics of PSC devices were obtained by a Keithley2400 SMU. Solar illumination conforming the JIS Class AAA was provided by a SAN-EI 300W solar simulator equipped with an AM 1.5G filter. The light intensity was calibrated with a Hamamatsu S1336-5BK silicon photodiode.

Transmission Electron Microscopy (TEM): TEM observations were performed in bright-field, high-resolution mode on a JEOL JEM-2010 transmission electron microscope with an accelerating voltage of 200 kV equipped with a Gatan-831 CCD camera. The thin-film sample was first spun-coated onto a ITO substrate covered with 40 nm of PEDOT:PSS. The sample was then immersed into water to dissolve the PEDOT:PSS layer and separate the thin films from the ITO substrate. Thin films floated on a water surface were picked up by copper grids coated with amorphous carbon layer, dried under vacuum overnight, and used in the TEM observations.

Synthesis of DTFBSe: To a round bottom flask was added 5,6-difluoro-4,7-diiodobenzo-2,1,3-selenadiazole (1.5 g, 3.18 mmol), $Pd(PPh_3)_4$ (290 mg, 0.251 mmol) and degassed DMF (50 mL). The solution was stirred at 60 °C until all the substance completely dissolved. 2-(tributylstannyl)thiophene (2.76 g, 7.4mmol) was added dropwise and the mixture was kept at 120 °C for 20 h. Then, the mixture was poured into water and extracted with dichloromethane, before being dried over anhydrous $MgSO_4$. After concentration, the residue was purified by column chromatography using hexane and dichloromethane (v/v = 4 : 1) as the eluent to afford an orange solid (0.66 g, yield 54%). ^{1}H NMR ($CDCl_3$, 400 MHz, δ): 7.27 (d, *J* = 4.8 Hz, 2H), 7.63 (d, *J* = 5.2 Hz, 2H), 8.18 (d, *J* = 4 Hz, 2H); ^{13}C NMR ($CDCl_3$, 75 MHz, δ): 112.38, 127.24, 129.04, 129.06, 129.08, 130.92, 130.97, 131.02, 131.70, 149.09, 149.31, 151.70, 151.92, 154.30; Anal. calcd for $C_{14}H_6F_2N_2S_2Se$: C 43.87, H 1.58, N 7.31; found: C 44.12, H 1.81, N 7.11.

Synthesis of 5,6-difluoro-4,7-bis(5-(trimethylstannyl)thiophen-2-yl)benzo-2,1,3-selenodiazole (A1): To a solution of compound DTFBSe (320 mg, 0.83 mmol) in dry THF (50 mL) was added a 2 M solution of lithium diisopropylamide in THF (1.08 mL, 2.16 mmol) dropwise at −78 °C. After stirring at −78 °C for 1 h, 1.0 M solution of chlorotrimethylstannane in THF (2.16 mL, 2.16 mmol) was introduced by syringe to the solution. The mixture solution was warmed up to room temperature and stirred for 20 h. The mixture solution was extracted with diethyl ether (50 mL ×3) and water (50 mL). Solvent was evaporated under reduced pressure and the product was obtained by recrystallization from methanol. Yield: 300 mg (51%) ^{1}H NMR ($CDCl_3$, 400 MHz, δ): 0.44 (s, 18H), 7.34 (d, *J* = 3.6 Hz, 2H), 8.22 (d, *J* = 3.6 Hz, 2H)

Synthesis of PTh$_4$FBSe: To a 50 mL round bottom flask was added, compound A1 (85.3 mg, 0.129 mmol), 5,5′-dibromo-4,4′-bis(2-octyldodecyl)-2,2′-bithiophene (D1) (114 mg, 0.129 mmol), tris(dibenzylideneacetone)dipalladium (5.9 mg, 0.0065 mmol), tri(2-methylphenyl)phosphine (15.7 mg, 0.052 mmol) and deoxygenated chlorobenzene (5 mL). The mixture was then degassed by bubbling nitrogen for 10 minutes at room temperature. The round bottom flask was put into the microwave reactor and heated to 180 °C under 270 watt for 50 minutes. Then, tributyl(thiophen-2-yl)stannane (10.5 mg, 0.028 mmol) was added to the mixture solution and reacted for 10 minutes under 270 W. Finally, 2-bromothiophene (20 mg, 0.123 mmol) was added to the mixture solution and reacted for 10 minutes under 270 W. After cooling to room temperature the solution was added dropwise to methanol. The precipitate was collected by filtration and washed by Soxhlet extraction with acetone (24 h) and hexane (24 h) sequentially. The residue solid was re-dissolved in hot toluene (100 mL). The Pd-thiol gel (Silicycle Inc.) was added to above toluene solution to remove the residual Pd catalyst at 60 °C for 12 h. After filtration of solution and removal of the solvent under reduced pressure, the polymer solution was added into methanol to re-precipitate. The purified polymer was collected by filtration and dried under vacuum for 1 day to give a black solid. Yield: 100 mg (50.2%). ^{1}H NMR ($CDCl_3$, 400 MHz, δ): 0.86 (br, 12H), 1.25 (br, 64H), 1.77 (br, 2H), 2.78 (br, 4H), 6.98-7.01 (br, 4H), 8.16 (br, 2H); Anal. calcd: C 67.29, H 8.02, N 2.53, S 11.59; found: C 66.76, H 7.34, N 2.66, S 11.75.

Synthesis of P1: Using a procedure similar to that described above for PTh$_4$FBSe, a mixture of A1 (43.04 mg, 0.06 mmol), A2 (40.2 mg, 0.06 mmol), D1 (107.5 mg, 0.12 mmol), tris(dibenzylideneacetone)dipalladium (5.56 mg, 0.0061 mmol), tri(2-methylphenyl)phosphine (14.8 mg, 0.049 mmol) in deoxygenated chlorobenzene (5 mL) was polymerized to give P1. Yield: 63 mg (47.8%). ^{1}H NMR ($CDCl_3$, 400 MHz, δ): 0.86 (br, 12H), 1.26 (br, 64H), 1.77 (br, 2H), 2.79 (br, 4H), 6.98-7.03 (br, 4H), 8.17-8.29 (br, 2H) Anal. calcd: C 68.75, H 8.19, N 2.59, S 13.32; found: C 67.24, H 7.50, N 2.81, S 13.35.

Synthesis of P2: Using a procedure similar to that described above for PTh$_4$FBSe, a mixture of A1 (18.52 mg, 0.026 mmol), A2 (51.88 mg, 0.078 mmol), D1 (92.85 mg, 0.104 mmol), tris(dibenzylideneacetone)dipalladium (5.56 mg, 0.0061 mmol), tri(2-methylphenyl)phosphine (14.8 mg, 0.049 mmol) in deoxygenated chlorobenzene (5 mL) was polymerized to give P2. Yield: 62 mg (55.1%). ^{1}H NMR ($CDCl_3$, 400 MHz, δ): 0.86 (br, 12H), 1.26 (br, 64H), 1.77 (br, 2H), 2.79 (br, 4H), 6.98-7.04 (br, 4H), 8.18-8.29 (br, 2H) Anal. calcd: C 69.53, H 8.28, N 2.61, S 14.25; found: C 69.48, H 7.84, N 2.80, S 14.44.

Results and Discussion

Synthesis and Thermal Analysis

As shown in Scheme 1, to obtain the FBSe alternating copolymer (PTh$_4$FBSe) and the FBSe:FBT ternary random copolymers (P1 and P2), the monomer 5,6-difluoro-4,7-bis(5-(trimethylstannyl)thiophen-2-yl)benzo-2,1,3-selenodiazole (A1) was first synthesized according to Scheme 1b. The Stille-coupling of 5,6-difluoro-4,7-diiodobenzo-2,1,3-selenodiazole and 2-(tributylstannyl)thiophene afforded the formation of DTFBSe in 68% yield. A1 was synthesized by reacting the lithiated DTFBSe with trimethyltin chloride in 54% yield. 5,6-difluoro-4,7-bis(5-(trimethylstannyl)thiophen-2-yl)benzo-2,1,3-thiadiazole (A2) and 5,5′-dibromo-4,4′-bis(2-octyldodecyl)-2,2′-bithiophene (D1) were synthesized via reported methods.[48] Then, PTh$_4$FBSe was synthesized by the copolymerization between A1 and D1 via Stille coupling. The ternary random copolymers, P1 and P2, were prepared by the copolymerization of the mixtures of A1, A2 and D1. The molar ratios were A1:A2:D1 = 1:1:2 for P1 and A1:A2:D1 = 1:3:4 for P2, respectively. The FBSe:FBT feed ratio of

PTh_4FBSe, P1 and P2 are thus 100:0, 50:50 and 25:75. The sulfur contains of the polymers from the elemental analysis are 11.75% for PTh_4FBSe, 13.35% for P1 and 14.25% for P2, respective. The contains closely match with the calculated values and give a clear indication about the FBSe:FBT ratios of the copolymers. The copolymers (PTh_4FBSe, P1 and P2) were completely soluble in chloroform, chlorobenzene (CB), and *o*-dichlorobenzene (*o*-DCB). The number average molecular weights (M_n) of PTh_4FBSe and P1 were 15.4 kDa (PDI = 1.72) and 12.3 kDa (PDI = 1.83), respectively, as determined by gel permeation chromatography (GPC). The molecular weight of P2 was not obtainable from GPC measurement due to its poor solubility in THF.

PTh_4FBSe, P1 and P2 exhibited good thermal stability with decomposition temperature (T_d) around 400 °C determined from thermogravimetric analysis (Fig. S2). In the DSC analysis (Fig. S3), the melting temperature (T_m) of PTh_4FBSe, P1 and P2 are 259 °C, 251 °C and 272 °C, respectively. The transition peaks of PTh_4FBSe and P2 are also sharper than that of P1. The different phase behaviors of the copolymers is related to the FBSe:FBT ratio. The highest T_m of P2 suggests that a higher FBT contain prompts the T_m of the copolymer. Moreover, the FBSe/FBT sequence along the conjugated backbone is non-negligible to the phase stability. Although P1 has a higher FBT ratio than PTh_4FBSe, its broad phase transition at lower temperature indicates that the backbone randomness decreases the transition temperature and the stability of the ordered phase.

Optical Absorption and Frontier Orbital Levels.

Fig. 1 displays the UV-Vis absorption spectra of the copolymers in *o*-DCB and thin film; Table 1 summarizes the optical data, including the absorption peak wavelengths (λ_{max}s), absorption edges (λ_{onset}s), and optical band gaps (E_gs) of the copolymers. In solution (Fig. 1a), the absorption bands at λ_{max} around 420 nm can be attributed to the localized π-π* transition and the absorption bands at λ_{max} around 580 nm were attributed to the photo-induced intramolecular charge transfer (ICT) between the electron-rich quaterthiophene units and electron-deficient FBT or FBSe units. As shown in Fig. 1b, the absorption bands bathochromically shift when the copolymers were spin-casted into the film. The low-energy absorption shoulders with λ_{max} located at 721 nm (PTh_4FBSe), 695 nm (P1) and 687 nm (P2) indicate a better backbone co-planarity and stronger intermolecular interactions of the conjugated chains in the thin film. The major influence of the FBSe:FBT ratio is on the E_g of

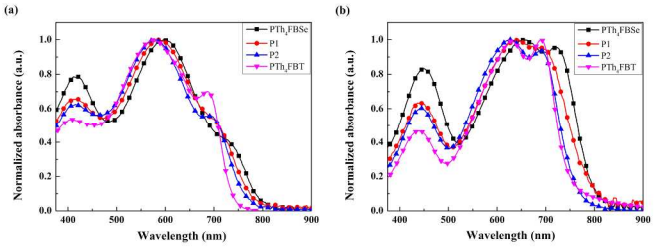

Fig. 1 Normalized (a) solution in *o*-DCB and (b) thin-film UV-vis absorption spectra of the copolymers.

the copolymer. Deduced from the absorption edges of the thin film spectra, the E_gs are 1.55 eV for PTh_4FBSe, 1.58 eV for P1 and 1.62 eV for P2, respectively. Thus, decrease of the FBSe content widens the E_g of the copolymers. The cyclic voltammetry (Fig. S1a) was performed for each copolymer to obtain information about their E_{HOMO} and E_{LUMO} levels. The relevant electrochemical properties are summarized in Table 1. Comparing the E_{HOMO}s and E_{LUMO}s of the copolymers, it was found that the decreased FBSe content drops the E_{HOMO}, but elevates the E_{LUMO} of the copolymers as shown in Fig. S1b. Thus, modulation of the E_{HOMO}s, E_{LUMO}s and E_gs of copolymers can be reached via the control of the FBSe:FBT ratio.

Table 1 Optical and electrochemical properties of copolymers

Polymer	λ_{max} (nm)		λ_{onset}	E_g	E_{HOMO}	E_{LUMO}
	Solution	Film	(nm)	(eV)	(eV)	(eV)
PTh_4FBSe	600	656, 721	798	1.55	5.27	3.80
P1	588	643, 695	791	1.57	5.31	3.72
P2	576	628, 687	761	1.62	5.35	3.70

X-ray Structural Characterization.

X-ray diffraction (XRD) analysis of the copolymers (Fig. 2) were carried out to identify how the FBSe:FBT ratio affects the solid-state packing of the copolymers. To give a comprehensive comparison, PTh_4FBT in our previous study[46] is also incorporated into the discussion. All copolymers form a long-range ordered lamellar structure (*d*-spacing of 2.07 nm), and ordered π−π stacking in the solid-state, as indicated by the three diffraction peaks indexed as the (100), (200), and (300) diffractions at low angle region, and the additional diffration at around 23.7° (*d*-spacing~ 0.37 nm). The π-π stacking distances ($d_{\pi-\pi}$s) are 0.374 nm for PTh_4FBSe and P2; 0.368 nm for P1; and 0.370 nm for PTh_4FBT.

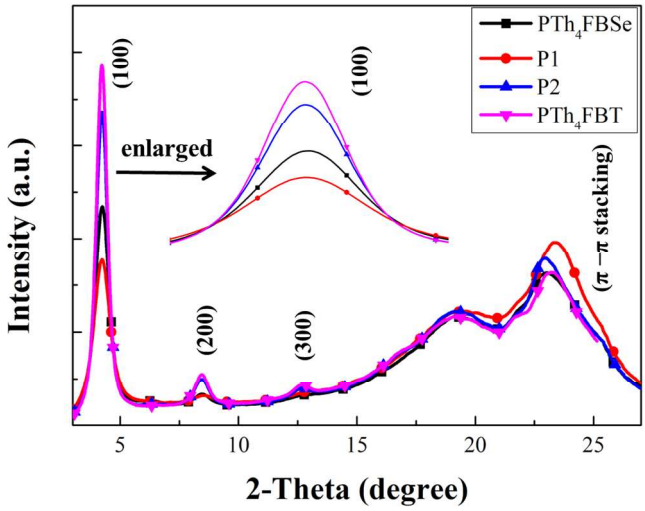

Fig. 2 Powder XRD patterns of the FBSe:FBT copolymers.

Fig. S5 shows the 2D WAXS pattern of the extruded samples. The chain axis (*c*-axis) of the copolymers is aligned along the shear direction. Therefore, the Bragg diffractions along the equator can be used to identify the diffractions from the lamellar structure (indexed as (100) in the figures), and the π−π stacking.[49] To make reasonable comparison, the sample diameter was controlled by the size of the pinhole on the extruder (1 mm) and the exposure time was fixed for the four samples. The scattering halo from the alkyl side chains was

clearly found at $2\theta = 19.2^{o}$ (d-spacing of 0.47 nm). Because the four polymers have the same alkyl side chains, the scattering intensities from the amorphous side chains are similar in the four diffraction patterns shown in Fig. S5. However, the integration of the diffraction peaks along the equator (Fig. S6) shows the differences in the diffraction intensities of the (100) and π-π peaks of the four copolymers. For the (100) diffraction, the intensities of the copolymers is in the order of PTh_4FBT >P2> PTh_4FBSe >P1 , and for the π-π diffraction, intensity is in the order of P1>P2> PTh_4FBSe ~ PTh_4FBT. The result is in accordance with the powder XRD patterns shown in Fig. 2. Thus, the XRD results indicate that the FBSe:FBT ratio does not affect the lamellar spacing, but does influence the order of the lamellar structure and the $d_{\pi-\pi}$ of the copolymers. Copolymers with higher FBT contains (PTh_4FBT and P2) generated sharper (100) diffractions than those with higher FBSe contains. Since the sharpness of the diffraction is related to the correlation length of crystalline domain according to the Scherrer equation, the order of the lamellar structure is therefore lower in the copolymers with higher FBSe contain (PTh_4FBSe) and higher backbone randomness (P1). However, to the π-stacking, the backbone randomness shows an opposite effect. The alternative copolymers - PTh_4FBSe and PTh_4FBT gave lower diffraction intensities for the π-π stacking than the random ternary copolymers - P1 and P2. Moreover, P1, which has the most random backbone, gave the most intense π-stacking diffraction and the shortest $d_{\pi-\pi}$ of 0.368 nm. Because the four copolymers are different in their FBSe:FBT ratio, or more specifically speaking, in the contain and the arrangement of the selenium (Se)/Sulfur (S) atoms, the result was rationale based on the steric effect of the Se atom and the intermolecular interaction strength of the FBSe unit. On the one hand, the atom size of Se is larger than S. Comparing the $d_{\pi-\pi}$ of PTh_4FBSe (0.374 nm) and PTh_4FBT (0.370 nm), it can be found that the larger atomic size of Se causes steric hindrance, and expands the $d_{\pi-\pi}$ of PTh_4FBSe.[50] On the other, due to the lower electronegativity of selenium, the FBSe unit actually possesses higher dipole moment (Fig. S4) for the stronger intermolecular interaction.[46] Therefore, in the case of P2, the low FBSe contain enhanced the interchain interaction and consequently increased the π-stacking diffraction intensity. The further increase in the FBSe contain, resulted in the even stronger π-stacking diffraction and shorter $d_{\pi-\pi}$ of P1. Therefore, the π-stacking order of the FBSe:FBT copolymers was affected both by the steric effect and the strength of the intermolecular interaction.

OFET Performances.

The charge transport properties of the FBSe:FBT copolymers were investigated in OFET devices with a bottom-gate, top-contact configuration. The output and transfer plots of the devices exhibitedtypical *p*-channel OFET characteristics (Fig. 3). The hole mobilities (μ_hs) of the copolymers were obtained from the transfercharacteristics of the devices in saturation regime. The μ_hs of PTh_4FBSe, P1 and P2 were 0.12, 0.46, and 0.32 $cm^2\ V^{-1}s^{-1}$, respectively. It was found that the μ_hs of the copolymers have better correlation to the π-stacking order than the lamellar order. P1, which has the highest π-stacking order and the shortest $d_{\pi-\pi}$, but the lowest lamellar order, delivered the highest μ_h (0.46 $cm^2\ V^{-1}s^{-1}$) among the copolymers. Remarkably, the μ_h of the random copolymer P1 is higher than the μ_hs of regular alternating copolymer, PTh_4FBSe (0.12 $cm^2\ V^{-1}s^{-1}$) and PTh_4FBT (0.29 $cm^2\ V^{-1}s^{-1}$).[46] The observation is not trivial, because it has been known that the lack of backbone regularity degraded the solid-state order and therefore the chargemobility of the conjugated polymers.[51] P1 provides an important example showing that although degrades the lamellar order, the adjustment of the FBSe:FBT ratio enables the optimization of the π-stacking order and the μ_hs of the copolymers.

Table2. OFET Characteristics of polymers.

Polymer	Annealing Temp. [°C]	Mobility [$cm^2\ V^{-1}s^{-1}$]	I_{on}/I_{off}	V_{th}[V]
PTh_4FBSe	200	0.12	9.19×10^5	-3.4
P1	200	0.46	1.24×10^7	-4.4
P2	250	0.32	9.19×10^6	-5.7

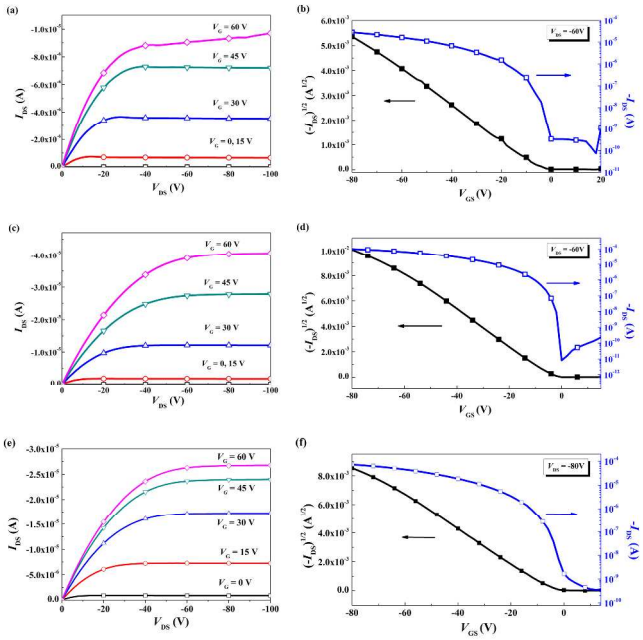

Fig3. Typical output curves (a, c, e) and transfer plots (b, d, f) of the OFET devices based on PTh_4FBSe, P1, and P2, respectively.

BHJ PSC Characteristics.

To evaluate the photovoltaic performances of the copolymers, BHJ PSCs with inverted architecture – ITO/ZnO/copolymer: $PC_{71}BM$ (1:2 w/w)/MoO_3/Ag were fabricated. The current density-voltage characteristics of the devices under a simulated AM 1.5 G illumination of 100 mW/cm^2 are show in Fig. 4 and summarized in Table 3. Without optimization, the V_{oc} and J_{sc} were 0.68 V, and 11.9 mA/cm^2 for the PTh_4FBSe PSCs; 0.68 V, and 11.4 mA/cm^2 for the P1 PSCs; and 0.72 V, and 10.5 mA/cm^2 P2 PSCs. The external quantum efficiency (EQE) measurements of the PSCs are shown in Fig. 5. Without DIO additive, PTh_4FBSe:$PC_{71}BM$ PSCs delivered the EQE value exceeds 40% over the wavelength range from 380 nm to 740 nm, but the EQE values of the P1:$PC_{71}BM$ and P2:$PC_{71}BM$ PSCs are lower in the same range. The results explain the highest J_{sc} of 11.9 mA/cm^2 delivered by the PTh_4FBSe:$PC_{71}BM$ PSCs. Although the EQE values of the P1:$PC_{71}BM$ and P2:$PC_{71}BM$ PSCs are similar in the wavelength range from 300 nm to 700 nm, the onset of the P2:$PC_{71}BM$ device is at 761 nm, but that of the

P1:$PC_{71}BM$ device is at 790 nm. The extra photons at longer wavelength region harvested by P1 contributed to the higher J_{sc} of the P1:$PC_{71}BM$ device. Thus, the higher FBSe contains in PTh_4FBSe and P1 led to the narrower E_gs of the copolymers and the higher J_{sc}s of the devices. On the contrary, the higher FBT contain of P2 resulted in the lower-lying E_{HOMO} and a higher V_{oc}.

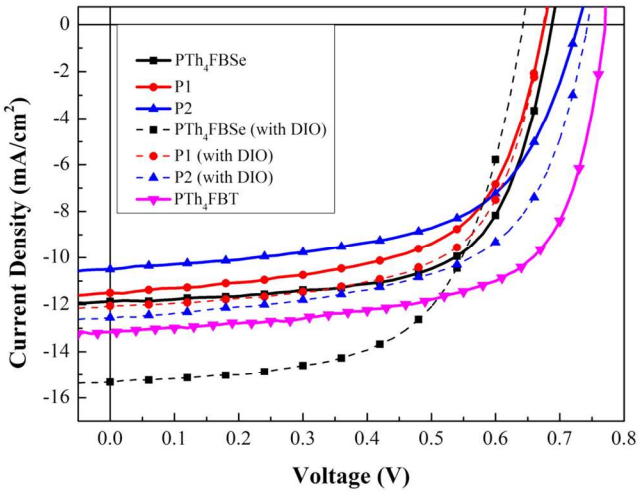

Fig. 4 Current density-voltage characteristics of the copolymer: $PC_{71}BM$ BHJ PSCs in inverted device architectures under illumination of AM 1.5 G at 100 mW/cm^2.

Table 3 PSCs Characteristics of the polymer: $PC_{71}BM$ BHJ PSCs

Polymer/$PC_{71}BM$ (w/w; 1 : 2)	V_{oc} (V)	J_{sc} (mA/cm^2)	*FF* (%)	PCE_{max}/PCE_{avg} [b] (%)
PTh_4FBSe	0.68	11.9	66.5	5.38/5.30
P1	0.68	11.4	60.5	4.70/4.54
P2	0.72	10.5	59.3	4.48/4.29
PTh_4FBSe [a]	0.64	15.3	61.8	6.06/6.04
P1[a]	0.68	12.0	64.1	5.20/5.16
P2[a]	0.74	12.6	60.6	5.63/5.56

[a] With 3 v% of DIO as additive
[b] The average value of 15 devices

However, when compared to the J_{sc} of PTh_4FBT:$PC_{71}BM$ PSCs (13.5 mA/cm^2),[46] the narrower E_g of PTh_4FBSe did not promote a higher J_{sc}. To identify the origins of the low J_{sc}, morphology of the active layers were investigated using HR-TEM. As shown in Fig. 5a, 5c, and 5e, the copolymer:$PC_{71}BM$ thin-films are very homogeneous, regardless the FBSe:FBT ratios of the copolymers. The images suggested that the copolymers have good miscibility to $PC_{71}BM$. These overly homogeneous blends may cause the insufficient phase separation and the fragmented charge transporting channels. Hence, DIO was used as process additive to promote the phase segregation.[52, 53] With 3 v% of DIO, the enhanced contrast in the PTh_4FBSe:$PC_{71}BM$ thin film (Fig. 5b) indicates an more obvious separation between PTh_4FBSe and $PC_{71}BM$. The interpenetrating PTh_4FBSe -rich, and $PC_{71}BM$-rich domains became relatively larger

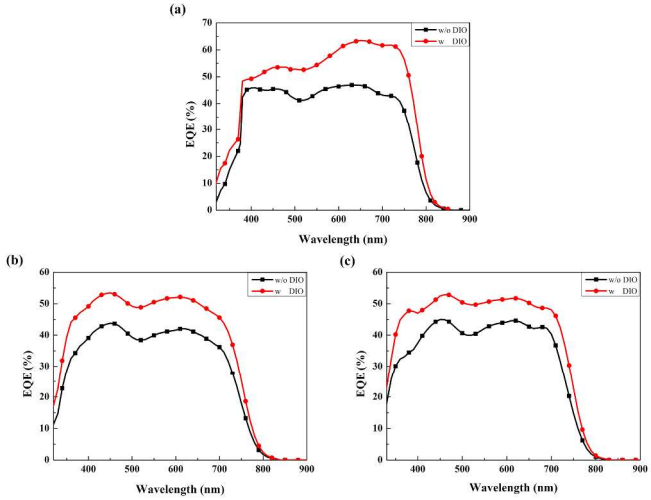

Fig. 5 External quantum efficiency (EQE) spectra of the (a) PTh_4FBSe:$PC_{71}BM$, (b) P1:$PC_{71}BM$, and (c) P2:$PC_{71}BM$ BHJ PSCs prepared with and without 3 v% of DIO.

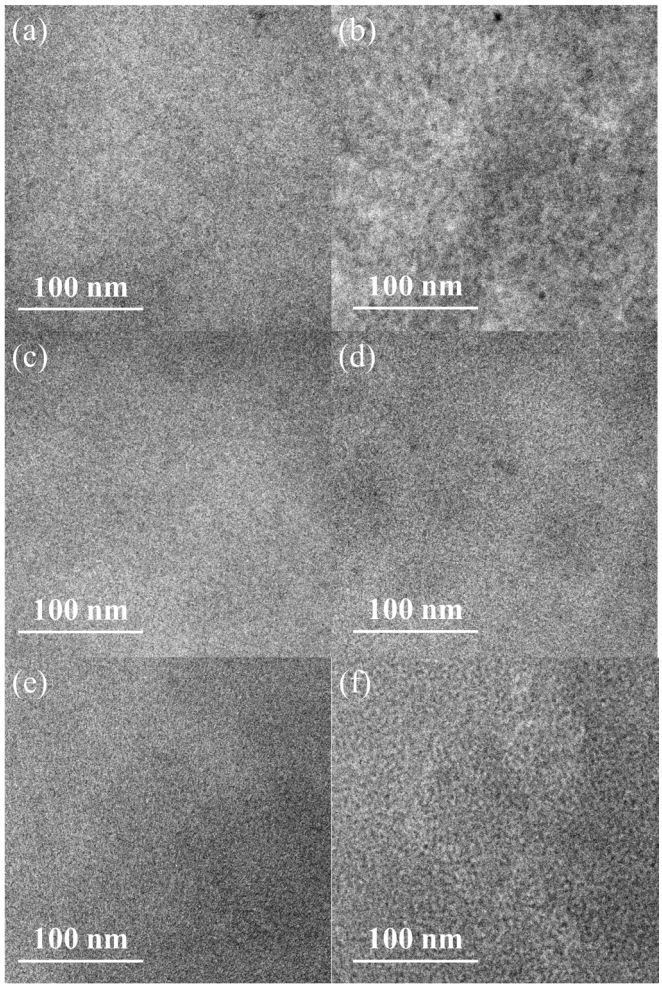

Fig. 6 HR-TEM images of (a) PTh_4FBSe:$PC_{71}BM$(1:2 in wt %) (b) PTh_4FBSe:$PC_{71}BM$(1:2 in wt %) with 3 v% of DIO (c) P1:$PC_{71}BM$(1:2 in wt %) (d) P1:$PC_{71}BM$(1:2 in wt %) with 3 v% of

DIO (e) P2:$PC_{71}BM$(1:2 in wt %) (f) P2:$PC_{71}BM$(1:2 in wt %) with 3 v% of DIO thin films prepared from a CB solution

and were beneficial for charge transport. The hole mobilities of the PTh_4FBSe:$PC_{71}BM$ blend films under a space charge limited current (SCLC) model increased from 6.73×10^{-4} $cm^2V^{-1}s^{-1}$ for the devices prepared without DIO to 3.38×10^{-3} $cm^2V^{-1}s^{-1}$ for those prepared with DIO, indicating that the enhanced phase separation improved the charge mobility. Furthermore, the EQE values of the PTh_4FBSe:$PC_{71}BM$ PSCs increased from 40% (Figure 5a, without DIO) to over 50% (Figure 5a, with DIO) in the wavelength range from 380 nm to 770 nm. Thus, because of the morphological change, the J_{sc} of the PTh_4FBSe:$PC_{71}BM$ PSCs (Fig. 5a) increased correspondly from 11.9 to 15.3 mA/cm^2 to give a PCE of 6.06%. However, DIO did not cause significant morphological changes in the P1:$PC_{71}BM$ and P2:$PC_{71}BM$ active layers as shown in the TEM images (Fig. 5d, 5f). It is possible that the random ternary copolymers have better miscibility to the $PC_{71}BM$, so that the DIO additive has less effect on the degree of phase separation. The J_{sc}s of the P1:$PC_{71}BM$ and P2:$PC_{71}BM$ PSCs increased slightly to 12.0 mA/cm^2 and 12.6 mA/cm^2, respectively, to deliver PCEs up to 5.20% and 5.63%.

Conclusions

In this study a series of D-A copolymers containing different FBSe:FBT ratio were synthesized. The influences of the FBSe:FBT ratio to the polymer properties, solid-state morphology and device performances were investigated. It was found that the copolymers with higher FBSe contains have narrower E_g, higher lying E_{HOMO}, and delivered higher J_{sc}, but lower V_{oc} in the PSCs. DSC results indicated that P1, which has the most irregular FBSe:FBT sequence along the backbone showed the lowest T_m. XRD results showed that the solid-state packing of the copolymers is affected by the chain sequence, steric effect of the chalcogen atoms (Se *vs.* S) and the intermolecular interaction strength. However, it is interesting to find that the irregularity in the chain sequence degrade the lamellar order, but not the π-stacking order. The random ternary copolymers, P1 and P2, possess more ordered π-stacking than the alternating copolymers, PTh_4FBSe and PTh_4FBT. The most irregular P1 even has the smallest $d_{\pi\text{-}\pi}$ among all the FBSe:FBT copolymers. Thus, P1 delivered the highest OFET μ_h of 0.46 cm^2 $V^{-1}s^{-1}$ because of its ordered π-stacking and small $d_{\pi\text{-}\pi}$. In the polymer:$PC_{71}BM$ blend films, the FBSe containing copolymers have good miscibility to $PC_{71}BM$. The degree of phase separation of PTh_4FBSe:$PC_{71}BM$ can be enhanced by DIO additive, but it is not effective for the random ternary copolymers. Highest PCE of 6.06% with V_{oc} of 0.64 V, J_{sc} of 15.3 mA/cm^2, and FF of 61.8% were delivered by the PTh_4FBSe:$PC_{71}BM$ PSCs. Because of the FBSe and FBT units are very similar in their structures, the influences of the acceptor ratios and the backbone randomness were better identified in this study.

Acknowledgements

This work is supported by the Ministry of Science and "ATP" project of the National Chiao Tung University and Ministry of Education, Taiwan.

Notes and references

Department of Applied Chemistry, National Chiao Tung University, 1001Ta Hsueh Rd., Hsinchu, Taiwan 30010

** Corresponding author: cshsu@mail.nctu.edu.tw; kclwang@nctu.edu.tw*

† Electronic Supplementary Information (ESI) available: [details of any supplementary information available should be included here]. See DOI: 10.1039/b000000x/

References

1. Y.-J. Cheng, S.-H. Yang and C.-S. Hsu, *Chem. Rev.*, 2009, **109**, 5868.
2. L. Lu and L. Yu, *Adv. Mater.*, 2014, **26**, 4413.
3. Y. Li, *Acc. Chem. Res.*, 2012, **45**, 723.
4. L. Dou, J. You, Z. Hong, Z. Xu, G. Li, R. A. Street and Y. Yang, *Adv. Mater.*, 2013, **25**, 6642.
5. J.-S. Wu, S.-W. Cheng, Y.-J. Cheng and C.-S. Hsu, *Chem. Soc. Rev.*, 2015, DOI: 10.1039/c4cs00250d.
6. H. Zhong, Z. Li, F. Deledalle, E. C. Fregoso, M. Shahid, Z. Fei, C. B. Nielsen, N. Yaacobi-Gross, S. Rossbauer, T. D. Anthopoulos, J. R. Durrant and M. Heeney, *J. Am. Chem. Soc.*, 2013, **135**, 2040.
7. S. Zhang, L. Ye, W. Zhao, D. Liu, H. Yao and J. Hou, *Macromolecules*, 2014, **47**, 4653.
8. Y.-X. Xu, C.-C. Chueh, H.-L. Yip, F.-Z. Ding, Y.-X. Li, C.-Z. Li, X. Li, W.-C. Chen and A. K.-Y. Jen, *Adv. Mater.*, 2012, **24**, 6356.
9. J. Subbiah, B. Purushothaman, M. Chen, T. Qin, M. Gao, D. Vak, F. H. Scholes, X. Chen, S. E. Watkins, G. J. Wilson, A. B. Holmes, W. W. Wong and D. J. Jones, *Adv. Mater.*, 2015, **27**, 702.
10. H. J. Son, L. Lu, W. Chen, T. Xu, T. Zheng, B. Carsten, J. Strzalka, S. B. Darling, L. X. Chen and L. Yu, *Adv. Mater.*, 2013, **25**, 838.
11. I. Osaka, T. Kakara, N. Takemura, T. Koganezawa and K. Takimiya, *J. Am. Chem. Soc.*, 2013, **135**, 8834.
12. C. B. Nielsen, R. S. Ashraf, N. D. Treat, B. C. Schroeder, J. E. Donaghey, A. J. P. White, N. Stingelin and I. McCulloch, *Adv. Mater.*, 2014, DOI: 10.1002/adma.201404858.
13. T. L. Nguyen, H. Choi, S. J. Ko, M. A. Uddin, B. Walker, S. Yum, J.-E. Jeong, M. H. Yun, T. J. Shin, S. Hwang, J. Y. Kim and H. Y. Woo, *Energy Environ. Sci.*, 2014, **7**, 3040.
14. J.-H. Kim, M. Lee, H. Yang and D.-H. Hwang, *J. Mater. Chem. A*, 2014, **2**, 6348.
15. Z. He, C. Zhong, S. Su, M. Xu, H. Wu and Y. Cao, *Nat. Photonics*, 2012, **6**, 591.
16. L. Dou, C.-C. Chen, K. Yoshimura, K. Ohya, W.-H. Chang, J. Gao, Y. Liu, E. Richard and Y. Yang, *Macromolecules*, 2013, **46**, 3384.
17. C.-Y. Chang, Y.-J. Cheng, S.-H. Hung, J.-S. Wu, W.-S. Kao, C.-H. Lee and C.-S. Hsu, *Adv. Mater.*, 2012, **24**, 549.
18. C. Cabanetos, A. El Labban, J. A. Bartelt, J. D. Douglas, W. R. Mateker, J. M. Frechet, M. D. McGehee and P. M. Beaujuge, *J. Am. Chem. Soc.*, 2013, **135**, 4656.
19. Y.-H. Chao, J.-F. Jheng, J.-S. Wu, K.-Y. Wu, H.-H. Peng, M.-C. Tsai, C.-L. Wang, Y.-N. Hsiao, C.-L. Wang, C.-Y. Lin and C.-S. Hsu, *Adv. Mater.*, 2014, **26**, 5205.
20. Z. Zhu, D. Waller, R. Gaudiana, M. Morana, D. Mühlbacher, M. Scharber and C. Brabec, *Macromolecules*, 2007, **40**, 1981.
21. J. Li, K.-H. Ong, P. Sonar, S.-L. Lim, G.-M. Ng, H.-K. Wong, H.-S. Tan and Z.-K. Chen, *Polym. Chem.*, 2013, **4**, 804.
22. K.-H. Kim, S. Park, H. Yu, H. Kang, I. Song, J. H. Oh and B. J. Kim, *Chem. Mater.*, 2014, **26**, 6963.
23. J. Zhou, S. Xie, E. F. Amond and M. L. Becker, *Macromolecules*, 2013, **46**, 3391.
24. P. Shen, H. Bin, L. Xiao and Y. Li, *Macromolecules*, 2013, **46**, 9575.
25. C. B. Nielsen, R. S. Ashraf, B. C. Schroeder, P. D'Angelo, S. E. Watkins, K. Song, T. D. Anthopoulos and I. McCulloch, *Chem. Commun.*, 2012, **48**, 5832.
26. T. E. Kang, H.-H. Cho, H. j. Kim, W. Lee, H. Kang and B. J. Kim, *Macromolecules*, 2013, **46**, 6806.
27. J. W. Jung, F. Liu, T. P. Russell and W. H. Jo, *Energy Environ. Sci*, 2013, **6**, 3301.
28. J.-M. Jiang, H.-C. Chen, H.-K. Lin, C.-M. Yu, S.-C. Lan, C.-M. Liu and K.-H. Wei, *Polym. Chem.*, 2013, **4**, 5321.
29. C.-H. Chen, Y.-J. Cheng, C.-Y. Chang and C.-S. Hsu, *Macromolecules*, 2011, **44**, 8415.
30. J.-S. Wu, J.-F. Jheng, J.-Y. Chang, Y.-Y. Lai, K.-Y. Wu, C.-L. Wang and C.-S. Hsu, *Polym. Chem.*, 2014, **5**, 6472.
31. M. Shahid, R. S. Ashraf, Z. Huang, A. J. Kronemeijer, T. McCarthy-Ward, I. McCulloch, J. R. Durrant, H. Sirringhaus and M. Heeney, *J. Mater. Chem.* , 2012, **22**, 12817.

32. H. A. Saadeh, L. Lu, F. He, J. E. Bullock, W. Wang, B. Carsten and L. Yu, *ACS Macro Lett.*, 2012, **1**, 361.
33. M. Planells, B. C. Schroeder and I. McCulloch, *Macromolecules*, 2014, **47**, 5889.
34. J. J. Intemann, K. Yao, H.-L. Yip, Y.-X. Xu, Y.-X. Li, P.-W. Liang, F.-Z. Ding, X. Li and A. K.-Y. Jen, *Chem. Mater.*, 2013, **25**, 3188.
35. L. Dou, W. H. Chang, J. Gao, C.-C. Chen, J. You and Y. Yang, *Adv. Mater.*, 2013, **25**, 825.
36. P. Shen, H. Bin, Y. Zhang and Y. Li, *Polym. Chem.*, 2014, **5**, 567.
37. Y. Li, Z. Pan, L. Miao, Y. Xing, C. Li and Y. Chen, *Polym. Chem.*, 2014, **5**, 330.
38. J.-H. Kim, S. A. Shin, J. B. Park, C. E. Song, W. S. Shin, H. Yang, Y. Li and D.-H. Hwang, *Macromolecules*, 2014, **47**, 1613.
39. R. Yang, R. Tian, J. Yan, Y. Zhang, J. Yang, Q. Hou, W. Yang, C. Zhang and Y. Cao, *Macromolecules*, 2005, **38**, 244.
40. J. Hou, M.-H. Park, S. Zhang, Y. Yao, L.-M. Chen, J.-H. Li and Y. Yang, *Macromolecules*, 2008, **41**, 6012.
41. G. L. Gibson, T. M. McCormick and D. S. Seferos, *J. Am. Chem. Soc.*, 2012, **134**, 539.
42. J.-M. Jiang, P. Raghunath, H.-K. Lin, Y.-C. Lin, M. C. Lin and K.-H. Wei, *Macromolecules*, 2014, **47**, 7070.
43. H. Zhou, L. Yang and W. You, *Macromolecules*, 2012, **45**, 607.
44. H. Zhou, L. Yang, A. C. Stuart, S. C. Price, S. Liu and W. You, *Angew. Chem.*, 2011, **50**, 2995.
45. A. C. Stuart, J. R. Tumbleston, H. Zhou, W. Li, S. Liu, H. Ade and W. You, *J. Am. Chem. Soc.*, 2013, **135**, 1806.
46. J.-F. Jheng, Y.-Y. Lai, J.-S. Wu, Y.-H. Chao, C.-L. Wang and C.-S. Hsu, *Adv. Mater.*, 2013, **25**, 2445.
47. E. Zhou, J. Cong, K. Hashimoto and K. Tajima, *Macromolecules*, 2013, **46**, 763.
48. K.-H. Ong, S.-L. Lim, J. Li, H.-K. Wong, H.-S. Tan, T.-T. Lin, L. C.-H. Moh, J. C. de Mello and Z.-K. Chen, *Polym. Chem.*, 2013, **4**, 1863.
49. C.-F. Huang, J.-Y. Chang, S.-H. Huang, K.-Y. Wu, J.-F. Jheng, W.-T. Chuang, C.-S. Hsu, C.-L. Wang, *J. Mater. Chem. A* 2015, ***3***, 3968-3974.
50. J. Hollinger, P. M. DiCarmine, D. Karl and D. S. Seferos, *Macromolecules*, 2012, **45**, 3772.
51. R. J. Kline, M. D. McGehee, E. N. Kadnikova, J. Liu and J. M. J. Fréchet, *Adv. Mater.*, 2003, **15**, 1519.
52. J. Peet, J. Y. Kim, N. E. Coates, W. L. Ma, D. Moses, A. J. Heeger and G. C. Bazan, *Nat. Mater.*, 2007, **6**, 497.
53. J. K. Lee, W. L. Ma, C. J. Barbec, J. Yuen, J. S. Moon, J. Y. Kim, K. Lee, G. C. Bazan and A. J. Heeger, *J. Am. Chem. Soc.*, 2008, **130**, 3619.

Table of Contents

Influences of the Backbone Randomness to the Properties, Morphology and Performances of the Fluorinated Benzoselenadiazole-Benzothiadiazole Based Random Copolymers

Yung-Tsung Chen, Tzu-Wei Huang, Chien-Lung Wang,* and Chain-Shu Hsu*

Random copolymerization has been developed as a versatile strategy to optimize the properties of D-A copolymers.

In this work, a series of fluorinated benzothiadiazole (FBT)-fluorinated benzoselenadiazole (FBSe) ternary random copolymers were synthesized. We studied that the copolymers' XRD behavior which affected the performance of OFET and OPVs.